Journal of ELECTRONIC MATERIALS, Vol. 38, No. 7, 2009
DOI: 10.1007/s11664-009-0698-2



# Synthesis of Nanocomposites with Improved Thermoelectric Properties

X.B. ZHAO,[1,2] S.H. YANG,[1] Y.Q. CAO,[1] J.L. MI,[1] Q. ZHANG,[1] and T.J. ZHU[1]

1.—State Key Laboratory of Silicon Materials, Department of Materials Science and Engineering, Zhejiang University, Hangzhou 310027, P.R. China. 2.—e-mail: zhaoxb@zju.edu.cn

Bulk thermoelectric materials are of interest for commercial application in both power generation and Peltier refrigeration. Various synthesis approaches have been developed by our group for high performance bulk thermoelectric materials, such as solvo- or hydrothermal synthesis for nanopowders, hot-pressing, and spark plasma sintering for nanostructured bulk materials, and rapid solidification for metal silicides. In this article we report some of our recent results in the development of high *ZT* thermoelectric materials, including $Bi_2Te_3$-$Sb_2Te_3$ nanocomposites and $CoSb_3$ micro/nanocomposites prepared by a powder blending route, and GeTe-$AgSbTe_2$ and $Mg_2Si$-$Mg_2Sn$ nanocomposites prepared by an *in situ* route. The results show various possibilities for improved microstructures and therefore enhanced properties of bulk thermoelectric materials through optimization of the preparation processing based on simple synthesis routes. A high *ZT* of approximately 1.5 has been obtained in both $Bi_2Te_3$-$Sb_2Te_3$ and GeTe-$AgSbTe_2$ nanocomposites. Further *ZT* enhancement of the materials should be possible through the control of the nanopowder morphology during synthesis and the hindering of grain growth during sintering, as well as through the optimization of composition and doping.

**Key words:** Thermoelectric materials, nanocomposites, bismuth tellurides, skutterudites, GeTe-$AgSbTe_2$ (TAGS) alloys, magnesium silicides

## INTRODUCTION

Nanostructuring is considered one of the most important approaches toward the attainment of high *ZT* values in bulk thermoelectric materials.[1] Theoretical[2] and experimental[3] results have shown that nanostructured low-dimensional materials possess a figure of merit *ZT* much higher than those of commercial bulk materials with similar compositions. Recent work has demonstrated that nanostructuring could also improve the *ZT* of bulk materials efficiently,[4–6] by reducing the thermal conductivity, $\kappa$, due to the boundary phonon scattering effect[7] and increasing the power factor, $\alpha^2\sigma$, due to the carrier confinement effect.[8] It has been suggested[9] that the so-called nano-effects in a bulk thermoelectric material could be remarkable only if some construction units (grains, particles, etc.) in the material were smaller than a few tens of nanometers or even a few nanometers, which is much smaller than features generally considered to be 'nano', i.e., approximately 100 nm.

The 10-nm structures imply a high density of boundaries and are, therefore, generally thermodynamically unstable. During heat treatment, module preparation and application at elevated temperatures, grain growth or particle coarsening would lead to a reduction of the nano-effects in a nanostructured material. There are, however, some techniques to hinder coarsening in nanostructures; for example, secondary nanoparticles may be added into the structure to block grain boundaries. It would be preferable if the secondary nanoparticles

(Received July 14, 2008; accepted January 29, 2009; published online February 24, 2009)

were also a thermoelectric material of the same conductive type as the matrix. Based on this requirement, we consider nanocomposites consisting of at least two thermoelectric components to be a promising way to improve the thermoelectric properties of a bulk material. It should be noted that all experimental results with $ZT > 2$ reported till now have been measured from nanocomposites with two thermoelectric (semiconducting) components, such as $Bi_2Te_3$-$Sb_2Te_3$ superlattice thin films with $ZT = 2.4$,[3] PbTe-$AgSbTe_2$ (LAST) with $ZT = 2.2$,[10] and PbTe-$PbSe_{0.98}Te_{0.02}$ quantum-dot superlattice with a possible $ZT$ value of 3.[11] The advantages of TE–TE nanocomposites are easily recognized. First, both components are thermoelectric materials and, therefore, contribute to the properties of the composite, while insulating nano-inclusions act like nano-pores. Secondly, the migration of a phase boundary is much slower than that of a grain boundary in a monophase material, since the former is related to the long-distance diffusion of atoms.

Two synthesis routes are available for the preparation of thermoelectric nanocomposites. One is the powder blending route, sintering a mixture of semiconducting powders to form bulk materials, and the other is the *in situ* route, producing nanostructures directly in a bulk material during heat processing. Here we show some of our recent work on high $ZT$ thermoelectric nanocomposites prepared by both routes.

## $Bi_2Te_3$ AND $CoSb_3$ BASED NANOCOMPOSITES OBTAINED BY THE POWDER BLENDING ROUTE

The most important advantage of the powder blending route is that one could produce composites simply by mixing the component powders to the designed ratios and sintering them together, with little care for the differences in the chemical and physical properties between the components. In order for 10 nm sized nanocomposites to be prepared, the sizes of the nanopowders, as the starting materials for sintering, should be as small as possible. In this work we used solvo- or hydrothermal synthesis to produce the nano-sized powders of both bismuth telluride based compounds[12,13] and $CoSb_3$ skutterudites.[14,15]

### $Bi_2Te_3$-$Sb_2Te_3$ Nanocomposites

Figure 1a shows the hydrothermally synthesized bismuth telluride nanopowders. Although various morphologies are possible, dependent upon the chemical composition of the material, the additives used, and the synthesis conditions, the typical sizes of the nanopowders are approximately 20 nm or smaller. Figure 1b is a transmission electron microscopy (TEM, JEOL-4000EX) photograph taken from the cross-plane of the disk sample NC11, hot-pressed from a 1:1 mixture of $Bi_2Te_3$ and $Sb_2Te_3$ nanopowders. The image in Fig. 1b shows a laminated structure composed of nano-layers with layer thicknesses between 5 nm and 50 nm.

The phase structures of the hot-pressed samples were investigated by x-ray diffraction (XRD) with a Rigaku D/MAX-2550P diffractometer using Cu $K_\alpha$ radiation ($\lambda = 1.54056$ Å). The in-plane and cross-plane XRD patterns of sample NC11 are plotted in (Fig. 2) and show a biphase structure consisting of both $Bi_2Te_3$ and $Sb_2Te_3$ phases. It should be noted that the differences between the in-plane and cross-plane XRD patterns are very small, implying negligible texture. This lack of texture suggests that the $Bi_2Te_3$ and $Sb_2Te_3$ layers in the hot-pressed sample were globally randomly oriented but exhibited small regions arranged in parallel, as shown in Fig. 1b. The results indicated that the bulk samples hot-pressed from the mixtures of $Bi_2Te_3$ and $Sb_2Te_3$ nanopowders were textureless nanocomposites composed of a layer thickness between 5 nm and 50 nm.

The electric conductivity $\sigma$ and the Seebeck coefficient $\alpha$ were measured with a computer-assisted device, described in our previous work.[16] The thermal conductivity $\kappa$ was calculated from the thermal diffusivity, the specific heat capacity and sample density were measured by laser flash (Netzsch LFA

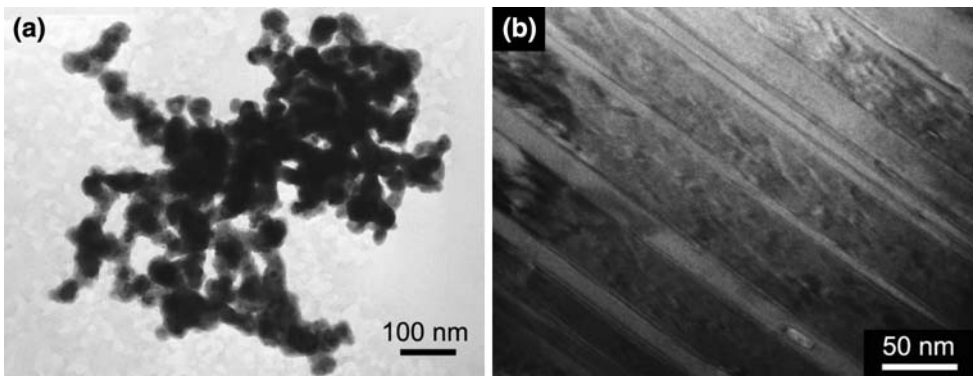


Fig. 1. TEM image of (a) the hydrothermally synthesized $Bi_2Te_3$ nanopowders and (b) disk NC11 hot-pressed from 1:1 mixture of $Bi_2Te_3$ and $Sb_2Te_3$.

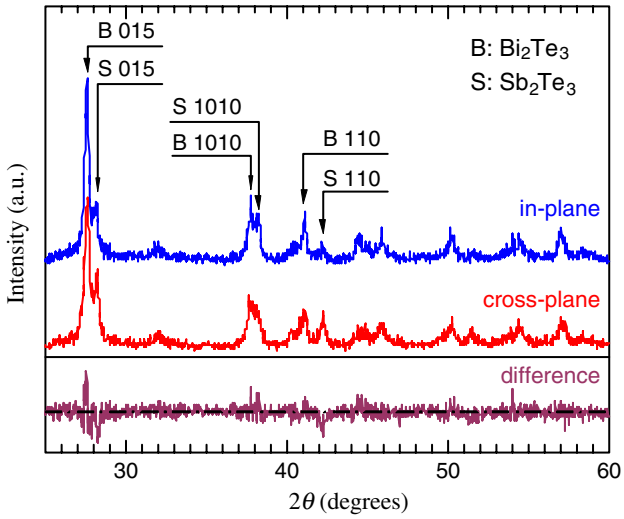


Fig. 2. XRD patterns of the hot-pressed disk NC11 taken both in-plane and cross-plane.

427), thermal analysis (Netzsch DSC 404), and Archimedes' method, respectively. The results are plotted in Fig. 3, where NC11 and NC13 are nanocomposite samples hot-pressed from 1:1 and 1:3 mixtures of $Bi_2Te_3$ and $Sb_2Te_3$, and MC11 and MC13 are microsized reference samples prepared by the same hot-pressing (HP) process and having the same chemical compositions as the nanocomposites but prepared with vacuum melted and ball milled micropowders of $Bi_2Te_3$ and $Sb_2Te_3$. Figure 3a shows that all samples are of *p*-type conduction. It should be noted that the nanocomposites possess not only a higher Seebeck coefficient but also a higher electric conductivity than the corresponding microsized composites. All nanocomposite samples exhibited lower thermal conductivities than those of the microcomposite samples, between 0.8 W (m K)$^{-1}$ and 1.4 W (m K)$^{-1}$ from room temperature to approximately 200°C, as shown in Fig. 3c. It is reasonable to suggest that the low thermal conductivity of the nanocomposites originates from the enhanced mid-to-long wave phonon scattering due to nanostructuring.[8] The highest dimensionless figure of merit *ZT* reached 1.47 for sample NC11, as shown in Fig. 3d. Since no dopant was used in any of the samples shown in Fig. 3, the *ZT* values of both microcomposite samples were rather low, making the effect of nanostructures even more significant. It could be expected that the properties of the nanocomposites could be further improved by doping optimization.

## $CoSb_3$ Based Micro/Nano-Composites

Figure 4a is a TEM photograph of the solvothermally synthesized $CoSb_3$ skutterudite nanopowders. Micropowders of Te-doped $CoSb_3$ were

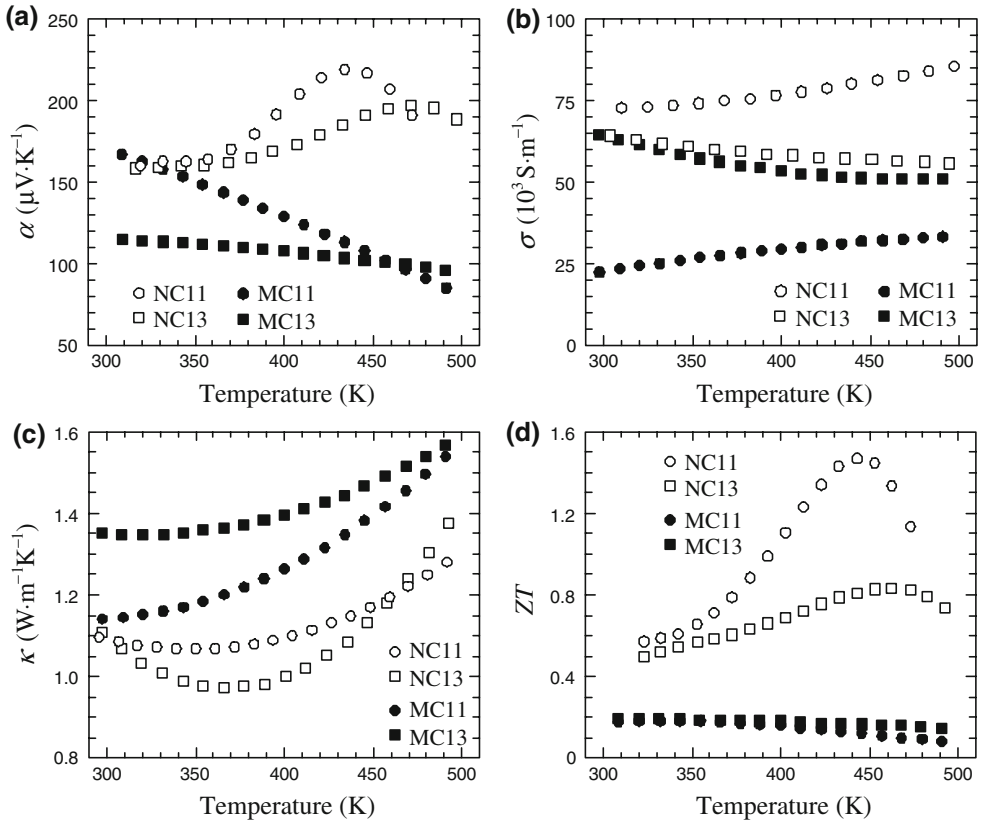


Fig. 3. Thermoelectric properties of the nanocomposites (NC11 and NC13) compared with the microsized composites (MC11 & MC13).

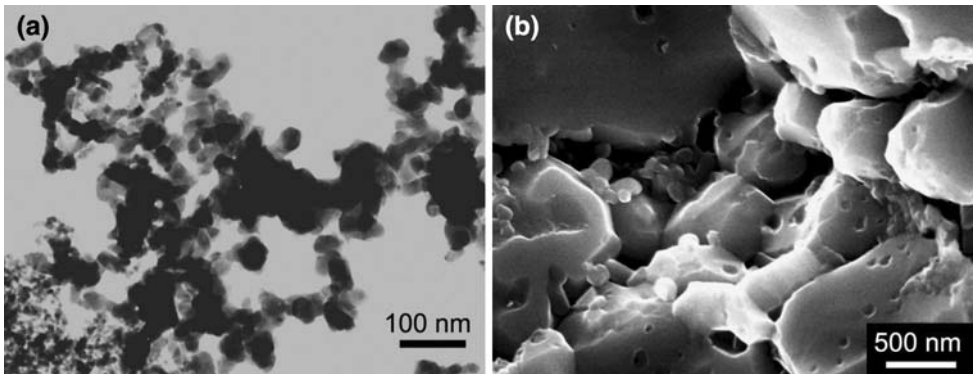


Fig. 4. (a) TEM photograph of the $CoSb_3$ nanopowders and (b) SEM image of the sample containing 5% nanopowder.

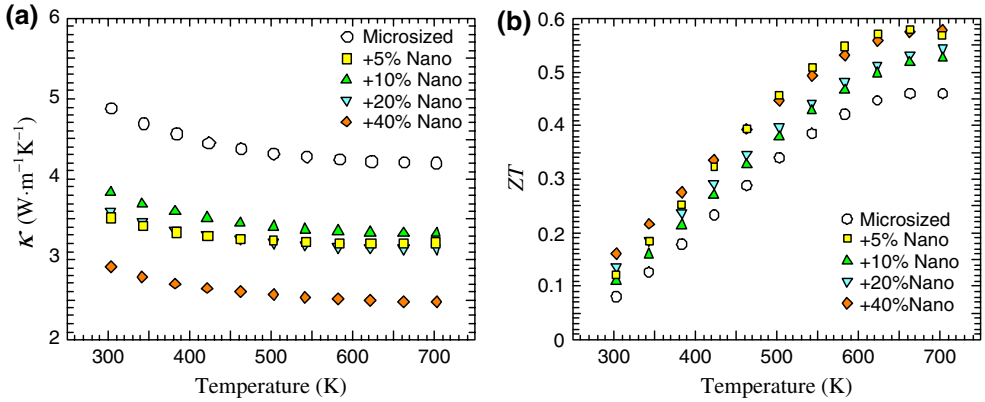


Fig. 5. (a) Thermal conductivities and (b) *ZT* of the $CoSb_3$ micro/nano-composites.

prepared by vacuum melting, vacuum annealing, and ball milling. Micro/nano-composite bulk samples were produced by the HP of the mixtures of micropowders and nanopowders. Figure 4b is a scanning electron microscopy (SEM) image of the fracture surface of the sample containing 5% nanopowder. We see that the nanoparticles were significantly coarsened from approximately 20 nm in Fig. 4a to about 100 nm after HP in Fig. 4b. The rapid coarsening of the nanopowders during HP could be due to the composition similarity between both nanopowder and micropowder, which allows particles to coarsen rapidly without long-distance diffusion of atoms.

The thermal conductivities and figures of merit of the $CoSb_3$-based composites are plotted in Fig. 5. The maximal *ZT* of the sample containing 5% nanopowder was approximately 0.58, which was about 25% higher than that of the sample without nano-additives, as shown in Fig. 5b. However, Fig. 5a illustrates that the improvement of *ZT* by nano-additives was mainly due to the reduction of thermal conductivity, which is approximately 25% for the sample containing 5% nanopowders in comparison with the microsized sample. For the samples with more nanopowder additives, the increases in *ZT* were even smaller than the decreases in $\kappa$. This means that the addition of nanopowders had no mentionable effects for enhancing the electric power factor $\alpha^2\sigma$. The reason could be the relatively large sizes of the nanocomponents in the composites.

If we compare this result with those obtained in the $Bi_2Te_3$-$Sb_2Te_3$ nanocomposite plotted in Fig. 3, we can recognize that the particle/grain sizes of a composite should be much smaller than 100 nm to reduce thermal conductivity by phonon confinement and enhance power factor by quantum effects at the same time, leading to the efficient improvement of the ZT in the composite.

## *IN SITU* FORMED GeTe-$AgSbTe_2$ AND $Mg_2Si$-$Mg_2Sn$ NANOCOMPOSITES

Even smaller domain sizes could be possible if nanocomposites were synthesized by an *in situ* route, when the nanostructures are formed directly in a bulk material. The *in situ* formed nanostructure could be manifested as solute-rich nanodomains such as those in $AgPb_mSbTe_{2+m}$,[10] or precipitated nanoparticles in a supersaturated solid solution such as those in $Bi_2Te_3$ alloyed with PbTe.[17]

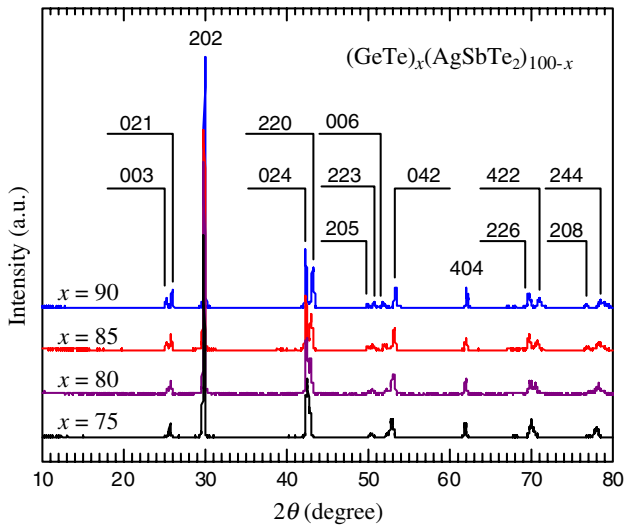


Fig. 6. XRD patterns of $(GeTe)_x(AgSbTe_2)_{100-x}$ ($x$ = 75, 80, 85, and 90).

## GeTe-$AgSbTe_2$ Nanocomposites

Samples with the designed compositions of $(GeTe)_x(AgSbTe_2)_{100-x}$ ($x$ = 75, 80, 85, and 90) were prepared by, in sequence: vacuum melting from the element metals in sealed quartz ampoules at 1000°C for 10 h, milling to powders with sizes $<150$ $\mu$m, and vacuum HP at 500°C under 70 MPa for 30 min. The XRD patterns showed that all GeTe-$AgSbTe_2$ (TAGS) samples were in rhombohedral GeTe-type phase with the space group *R3m* (JCPDF No. 47-1079). With increasing content of $AgSbTe_2$ the (024) peak shifts left and (220) shifts right, tending to overlap, behaving as typical solid solutions of GeTe and $AgSbTe_2$ (Fig. 6).

The grain sizes of the hot-pressed TAGS samples were generally in the sub-micrometer range, but grains of a few tens of nanometers could also be found, as shown in Fig. 7a. Also noted in Fig. 7a are nanosized inhomogeneous dots embedded within grains. The high-resolution transmission electron microscopy (HRTEM) photograph in Fig. 7b indicates that most of these nanodots have the same crystal orientation as the surrounding grain, but there are also differently oriented nanodomains, as shown in the inserted photograph in Fig. 7b. These nanodots or nanodomains of only a few nanometers could be observed throughout the TAGS samples except the low $AgSbTe_2$ sample with $x$ = 90, suggesting that these nanostructures originated from the composition fluctuation of AgSb in the microstructure and formed *in situ* during the heat processing of the material. Similar nanostructures have been observed in $AgSbTe_2$-PbTe and $AgSbTe_2$-SnTe systems.[18–20] The nanodots could act as potential barriers for intermediate frequency phonons and carriers.[8]

From the measured data of power factors, $\alpha^2\sigma$, and thermal conductivities, $\kappa$, of the $(GeTe)_x(AgSbTe_2)_{100-x}$ samples plotted in Fig. 8, it should be noted that samples with high AgSb content ($x \le 85$) possess higher $\alpha^2\sigma$ and lower $\kappa$ values at the same time than the sample of $x$ = 90. Considering the fact that a proper high AgSb content is favorable for the formation of nanodomains in TAGS alloys, as observed in this work, it could be concluded that the high density of nanodomains with sizes of only a few nanometers are crucial to increasing the power factor and reducing the thermal conductivity coinstantaneously in the materials. The maximal $ZT$ calculated from the data given in Fig. 8 reached over 1.5 at 720 K for the samples with $x \le 85$, much higher than that of the sample with $x$ = 90.

## $Mg_2Si$-$Mg_2Sn$ Nanocomposites

Sb-doped $Mg_2Si$-$Mg_2Sn$ bulk materials with the composition of $Mg_2Si_{0.4-x}Sn_{0.6}Sb_x$ ($x$ = 0, 0.002, 0.005, 0.0075, 0.010, 0.015) were prepared by vacuum melting, milling, HP at 700°C for 2 h, followed by natural cooling to room temperature. XRD patterns plotted in Fig. 9 show that all samples exhibited features of monophase $Mg_2Si$-$Mg_2Sn$ solid solutions.

However, in the TEM photograph, Fig. 10a, one sees a number of 'particles' with different contrasts and sizes, from a few nanometers to a few tens of nanometers. From the high-resolution image,

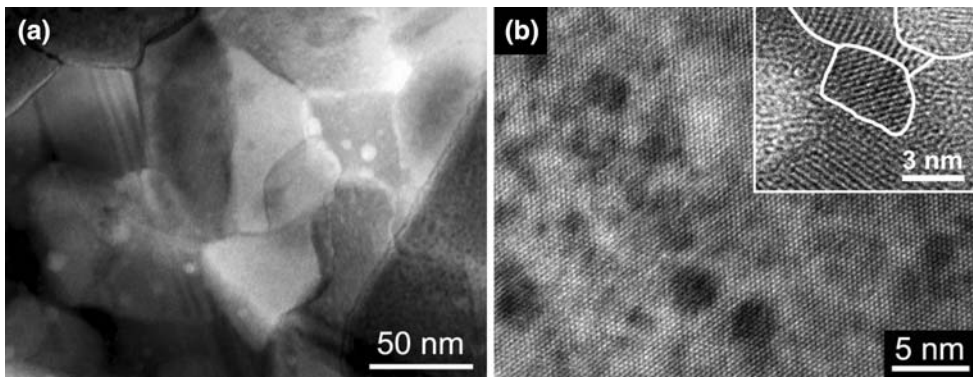


Fig. 7. (a) TEM and (b) HRTEM photographs of $(GeTe)_{80}(AgSbTe_2)_{20}$.

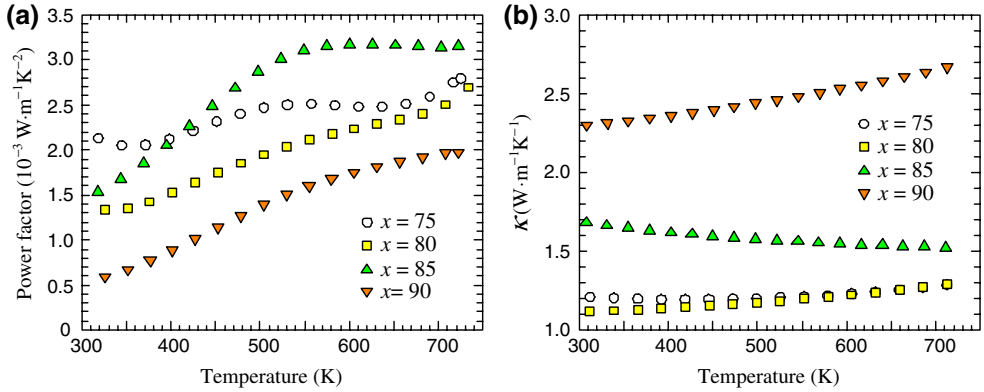


Fig. 8. (a) Power factor and (b) thermal conductivity of the $(GeTe)_x(AgSbTe_2)_{100-x}$ samples.

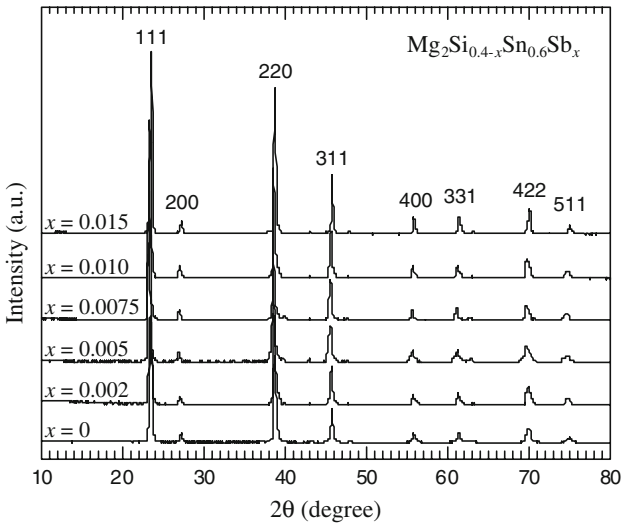


Fig. 9. XRD patterns of the hot-pressed $Mg_2Si_{0.4-x}Sn_{0.6}Sb_x$ samples.

Fig. 10b, we see that they are embedded nanodomains with orientations different from that of the surrounding grain. The large surrounding grain in Fig. 10b is clearly a single grain, since neither orientation difference nor visible inner grain boundaries can be found in the large grain. The compositions of the nanodomains should be different from that of the large grain, because an inner nanograin with the same composition as its surrounding would rapidly disappear during the heat processing. Hence, the material is believed to be an *in situ* nanocomposite containing Si-rich nanodomains embedded in Sn-rich micrograins. The high-density and randomly distributed nanodomains in the $Mg_2Si$-$Mg_2Sn$ alloy are expected to enhance the scattering of both carriers and phonons favorably, therefore improving the thermoelectric figure of merit of the nanocomposites.

Figure 11 shows the thermoelectric properties of the Sb-doped $Mg_2Si_{0.4}Sn_{0.6}$ samples. It is noted from Fig. 11a that the electric conductivity increases with the dopant amount of Sb from $x = 0$ to 0.0075 and then decreases when $x > 0.0075$, suggesting that the solubility of Sb in $Mg_2Si_{0.4}Sn_{0.6}$ is approximately 0.0075 mole per mole $Mg_2Si_{0.4}Sn_{0.6}$. From the data in Fig. 11, it can be calculated that the sample with $x = 0.0075$ possesses the highest $\sigma/\kappa$ ratio and lowest phonon conductivities $\kappa_{ph} = \kappa - L_0T$ ($L_0 = 2.44 \times 10^{-8}$ V$^2$ K$^{-2}$ for degenerate semiconductors) among all samples. A high $ZT$, over 1, was obtained in this work from samples doped with 0.005 and 0.0075 mole Sb per mole $Mg_2Si_{0.4}Sn_{0.6}$ at approximately 700 K.

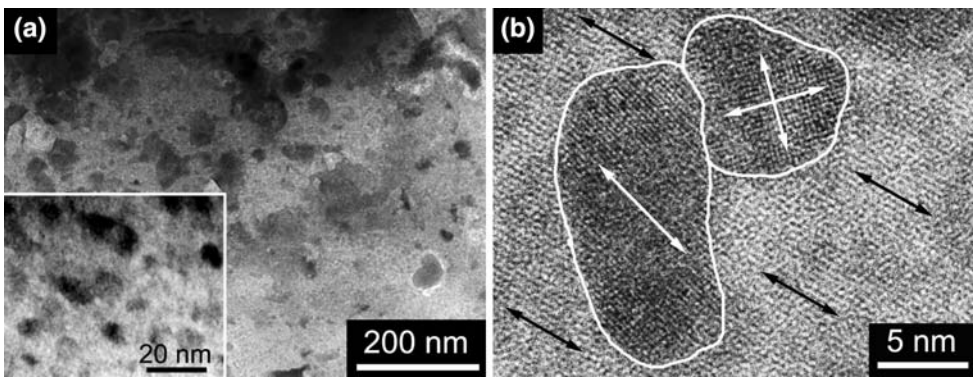


Fig. 10. (a) TEM and (b) HRTEM photographs of the $Mg_2Si_{0.4-x}Sn_{0.6}Sb_x$ sample ($x = 0.0075$).

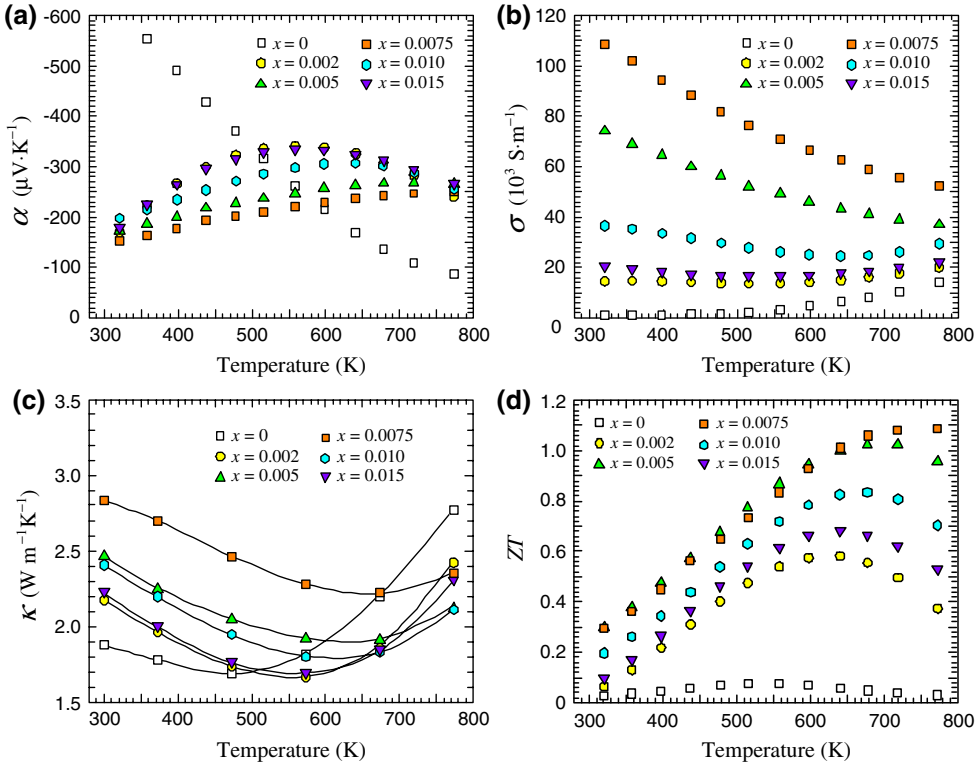


Fig. 11. Thermoelectric properties of the $Mg_2Si_{0.4-x}Sn_{0.6}Sb_x$ samples.

## CONCLUSIONS

Thermoelectric nanocomposites were synthesized by sintering the mixture of semiconducting powders to bulk materials, the powder blending route, or by forming nanostructures directly in a bulk material during heat processing, the *in situ* route, for various thermoelectric materials. Nanocomposites with particle sizes of a few tens of nanometers can be produced by the powder blending route using solvothermally/hydrothermally synthesized nanopowders. However, rapid coarsening would also be possible if the powders were similar in chemical composition. Nanocomposites with even finer nanostructures of only a few nanometers can be obtained if the *in situ* route can be used in a particular material, whereby nanoparticles are directly formed in the bulk material during heat processing. Both routes are simple and suitable to produce thermoelectric bulk nanocomposites with high thermoelectric properties.

## ACKNOWLEDGEMENTS

The work is supported by the "973" Program of China (2007CB607502), Natural Science Foundation of China (50731006, 50601022, 50522203), the "863" Program of China (2007AA03Z234), and the DPHE of the Ministry of Education of China (20060335126).

## REFERENCES

1. M.S. Dresselhaus, G. Chen, M.Y. Tang, R.G. Yang, H. Lee, D.Z. Wang, Z.F. Ren, J.P. Fleurial, and P. Gogna, *Adv. Mater.* 19, 1043 (2007). doi:10.1002/adma.200600527.
2. X. Sun, Z. Zhang, and M.S. Dresselhaus, *Appl. Phys. Lett.* 74, 4005 (1999). doi:10.1063/1.123242.
3. R. Venkatasubramanian, E. Siivola, T. Colpitts, and B. O'Quinn, *Nature* 413, 597 (2001). doi:10.1038/35098012.
4. X.F. Tang, W.J. Xie, H. Li, W.Y. Zhao, Q.J. Zhang, and M. Niino, *Appl. Phys. Lett.* 90, 012102 (2007). doi:10.1063/1.2425007.
5. B. Poudel, Q. Hao, Y. Ma, Y.C. Lan, A. Minnich, B. Yu, X. Yan, D.Z. Wang, A. Muto, D. Vashaee, X.Y. Chen, J.M. Liu, M.S. Dresselhaus, G. Chen, and Z. Ren, *Science* 320, 634 (2008). doi:10.1126/science.1156446.
6. Y.Q. Cao, X.B. Zhao, T.J. Zhu, X.B. Zhang, and J.P. Tu, *Appl. Phys. Lett.* 92, 143106 (2008). doi:10.1063/1.2900960.
7. R.G. Yang, G. Chen, and M.S. Dresselhaus, *Phys. Rev. B* 72, 125418 (2005). doi:10.1103/PhysRevB.72.125418.
8. W. Kim, J. Zide, A. Gossard, D. Klenov, S. Stemmer, A. Shakouri, and A. Majumdar, *Phys. Rev. Lett.* 96, 045901 (2006). doi:10.1103/PhysRevLett.96.045901.
9. X.B. Zhao, X.H. Ji, Y.H. Zhang, T.J. Zhu, J.P. Tu, and X.B. Zhang, *Appl. Phys. Lett.* 86, 062111 (2005). doi:10.1063/1.1863440.
10. K.F. Hsu, S. Loo, F. Guo, W. Chen, J.S. Dyck, C. Uher, T. Hogan, E.K. Polychroniadis, and M.G. Kanatzidis, *Science* 303, 818 (2004). doi:10.1126/science.1092963.
11. T.C. Harman, M.P. Walsh, B.E. Laforge, and G.W. Turner, *J. Electron. Mater.* 34, L19 (2005). doi:10.1007/s11664-005-0083-8.
12. X.B. Zhao, X.H. Ji, Y.H. Zhang, G.S. Cao, and J.P. Tu, *Appl. Phys. A* 80, 1567 (2005). doi:10.1007/s00339-004-2956-8.
13. X.B. Zhao, T. Sun, T.J. Zhu, and J.P. Tu, *J. Mater. Chem.* 15, 1621 (2005). doi:10.1039/b500759c.

14. J.L. Mi, X.B. Zhao, T.J. Zhu, J.P. Tu, and G.S. Cao, *J. Alloys Compd.* 417, 269 (2006). doi:10.1016/j.jallcom.2005.09.033.
15. J.L. Mi, X.B. Zhao, T.J. Zhu, J.P. Tu, and G.S. Cao, *J. Alloys Compd.* 399, 260 (2005). doi:10.1016/j.jallcom.2005.03.013.
16. J.L. Mi, T.J. Zhu, X.B. Zhao, and J. Ma, *J. Appl. Phys.* 101, 054314 (2007). doi:10.1063/1.2436927.
17. D.G. Ebling, A. Jacquot, M. Jagle, H. Bottner, U. Kuhn, and L. Kirste, *Phys. Status Solidi Rapid Res. Lett.* 1, 238 (2007).
18. E. Quarez, K.F. Hsu, R. Pcionek, N. Frangis, E.K. Polychroniadis, and M.G. Kanatzidis, *J. Am. Chem. Soc.* 127, 9177 (2005). doi:10.1021/ja051653o.
19. J. Androulakis, C.H. Lin, H.J. Kong, C. Uher, C.I. Wu, T. Hogan, B.A. Cook, T. Caillat, K.M. Paraskevopoulos, and M.G. Kanatzidis, *J. Am. Chem. Soc.* 129, 9780 (2007). doi:10.1021/ja071875h.
20. J. Androulakis, K.F. Hsu, R. Pcionek, H. Kong, C. Uher, J.J. Dangelo, A. Downey, T. Hogan, and M.G. Kanatzidis, *Adv. Mater.* 18, 1170 (2006). doi:0.1002/adma.200502770.